Fourth International Conference on CFD in the Oil and Gas, Metallurgical & Process Industries
SINTEF / NTNU Trondheim, Norway
6-8 June 2005

2D SIMULATIONS OF BUBBLING GAS-SOLID FLUIDIZED BED REACTORS

Håvard LINDBORG and Hugo A. JAKOBSEN

[1] NTNU Department of Chemical Engineering, 7491 Trondheim, NORWAY

ABSTRACT

This paper discusses the simulation of bubbling gas-solid flows by using an Eulerian modeling approach. Two closure models, the constant particle viscosity model (CPV) and a model based on kinetic theory of granular flow (KTGF), are compared in performance to describe the time-averaged velocity fields and bed expansion in both a circular and rectangular column. The time averaged velocity fields and bed expansion obtained in the simulations are compared with experimental data obtained by Lin et al. (1985) for validation.

In this work an in-house code has been developed based on the finite volume and the fractional step approach using a staggered grid arrangement. The velocities in both phases are obtained by solving the two-dimensional Reynolds-averaged Navier/Stokes equations using a partial elimination algorithm (PEA) and a coupled solver. The k-epsilon turbulence model is used for the continuous phase.

Axi-symmetric simulations using the KTGF model gives results in fairly well agreement with the experimental results, while the CPV model predicts unrealistically high solids concentration along the central axis due to the symmetry condition. Applying higher order discretizations of the convective terms results in a higher solids void fraction as long as the diffusion in the system is sufficiently high.

The first step of including a chemical reactive system seems to be successful, although validation of the chemical process still remains.

Keywords: Bubbling bed reactors; Fluid Mechanics; Multiphase flow; Simulation; Viscous flow; CFD;

NOMENCLATURE

D_{ea} *d*ispersion coefficient
$\mathbf{M}_k$ interfacial momentum transfer term
e restitution coefficient
g gravity vector
g_0 radial distribution function
p pressure
$\mathbf{v}_k$ velocity
R_j reaction rate

Γ_d conductivity of solid phase fluctuating energy
α_k void fraction of phase k
β *d*rag coefficient
γ collisional energy dissipation
ζ_d solid phase bulk viscocity
θ granular temperature
μ_d^{dilute} dilute viscosity
ρ_k intrinsic density of phase k
μ dynamic viscosity
τ_k Stress of phase k
ω_i species mass fraction

INTRODUCTION

The Eulerian modeling approach is probably the most commonly used approach for predicting the dynamical behavior in fluid-particle systems (for example Enwald et al., 1996, van Wachem et al., 1998). This approach describes both phases as interpenetrating continua and has more potential, compared to an Euler-Lagrangian approach, in situations where the dynamics of the system is of interest or the mass-loading of the dispersed phase is considerable. However, many Euler-Euler models used in the literature suffer from uncertainties in prescribing the internal momentum transfer in the solid phase (Ding and Gidaspow, 1990). Various non-Newtonian models for the internal stresses of the solid phase correlated with experimental observations have been proposed. In recent years, more fundamental closures for these stresses have been developed based on the application of the kinetic theory for dense gases to particulate assemblies. The work of Ding and Gidaspow (1990), Samuelsberg and Hjertager (1996) and Laux (1998) among others have shown the ability of the Euler-Euler granular temperature approach to model, numerically, gas-solid fluidized beds. In this work two closure models, the classical constant particle viscosity model (CPV) and a more fundamental model based on kinetic theory of granular flow (KTGF), are compared in performance to describe the time-averaged velocity fields and bed expansion in both a circular and rectangular column. The former model can be considered as a simplification of the latter, where a uniform and constant granular temperature in the entire fluidized bed is assumed.

The motivation for this work is to describe reactive flows in fluidized bed reactors and thereby couple the fluid dynamic models with a chemical reaction model containing complex reaction kinetics and chemical equilibriums. In a first step of this description, the chemical system chosen is the synthesis gas process for hydrogen production.

Hydrogen is an important raw material in chemical and petroleum industries. However, the importance of hydrogen is believed to increase as it might become a new generation of clean energy source for transport, as it can be applied in combustion processes as well as in the fuel cell technology. In that case, the hydrogen demand is expected to increase drastically. Steam reforming is currently the major process for large-scale production of hydrogen. An alternative cost-effective process for hydrogen production is highly desirable as traditional steam reforming includes multiple processing steps and severe operating conditions, making the hydrogen production very costly.

Sorption enhanced reaction process (SERP) is a multifunctional reactor concept suitable as an alternative to traditional steam reforming. The concept is a combination of reaction and separation where a CO_2 acceptor can be installed together with the catalyst to remove CO_2 from the gas phase. High fractions of hydrogen can be obtained as the normal equilibrium limits of reforming and shift reaction practically vanish. In addition, the process can be operated at much lower temperatures which will significantly lower investment and operation costs. Lower temperatures and lower concentration of CO in addition to higher concentration of hydrogen will also reduce the cocking potential, which is a serious problem in traditional steam reforming.

As the SERP-concept involves regeneration of the sorbent in which CO_2 is removed, a fluidized bed might be a suitable choice of reactor for this process. The well-known advantages of the fluidized bed concept as continuous sorbent regeneration, small temperature gradients as well as small mass transfer resistance are favorable in SERP.

The SERP-concept will be included in the models forthwith as the kinetics of this process is known.

MODEL DESCRIPTION

In this section the governing and constitutive equations for the two-fluid model are presented, along with the associated boundary conditions.

Governing equations

For simulation of the bubbling gas-solid flows an Eulerian modeling approach has been applied. The conservation equations for mass, momentum, granular energy and species composition are given in Table 1.

Continuity equation for phase k (=c, d):

$$\frac{\partial}{\partial t}(a_k r_k) + \nabla\cdot(a_k r_k \mathbf{v}_k) = 0 \qquad (1)$$

Momentum equation for phase k (=c, d):

$$\frac{\partial}{\partial t}(a_k r_k \mathbf{v}_k) + \nabla\cdot(a_k r_k \mathbf{v}_k \mathbf{v}_k) = -a_k \nabla p + \nabla\cdot\bar{\boldsymbol{\tau}}_k + a_k r_k \mathbf{g}_k + \mathbf{M}_k \qquad (2)$$

Granular temperature:

$$\frac{3}{2}\left[\frac{\partial}{\partial t}(a_d r_d \Theta) + \nabla\cdot(a_d r_d \mathbf{v}_d \Theta)\right] = \bar{\boldsymbol{\tau}}_d : \nabla \mathbf{v}_d + \nabla\cdot(\Gamma_d \nabla\Theta) - 3\beta\Theta - \gamma \qquad (3)$$

Species composition:

$$\frac{\partial}{\partial t}(a_c r_c w_i) + \nabla\cdot(a_c r_c \mathbf{v}_c w_i) = \nabla\cdot(a_c r_c D_{ea} \nabla w_i) + R_j \qquad (4)$$

Table 1 Governing conservative equations.

Constitutive equations

Constitutive equations for modeling interfacial momentum transfer are given in Table 2. The drag force is expected to be the most dominant interfacial force for particle flows. It is here represented by the Ergun equation for the dense regime (Ergun; 1952), while a correlation of Wen and Yu (1966) is applied for the dilute regime. A linear combination of the two drag formulations is applied in the transition regimes.

Interfacial force

$$\mathbf{M}_c = -\mathbf{M}_d = \mathbf{F}_D = \beta(\mathbf{v}_d - \mathbf{v}_c) \qquad (5)$$

Interfacial friction coefficient:

$$\beta = \frac{3}{4 d_d} a_d a_c r_c C_D |\mathbf{v}_d - \mathbf{v}_c| a_c^{-2.65} \psi + 150\frac{a_d^2 \mu_c}{a_c d_d^2} + 1.75\frac{a_d r_c |\mathbf{v}_d - \mathbf{v}_c|}{d_d}(1-\psi) \qquad (6)$$

Dragcoefficient:

$$C_D = \begin{cases} \dfrac{24}{\mathrm{Re}_p}\left(1 + 0.15\,\mathrm{Re}_p^{0.687}\right) & \text{if } \mathrm{Re}_p < 1000 \\ 0.44 & \text{if } \mathrm{Re}_p \geq 1000 \end{cases}$$

Weight function:

$$\psi = \begin{cases} 1 & \text{if } a_c > 0.825 \\ \dfrac{a_c - 0.775}{0.825 - 0.775} & \text{if } 0.825 \geq a_c > 0.775 \\ 0 & \text{if } a_c \leq 0.775 \end{cases}$$

Reynolds number:

$$\mathrm{Re}_p = \frac{a_c r_c |\mathbf{v}_d - \mathbf{v}_c| d_d}{\mu_c}$$

Table 2 Constitutive equations applied in the two-fluid model.

Constant particle viscosity model

As the name implies the CPV model does not contain any viscosity model. The stress tensor of the solid phase is then given by equation (10) where the bulk viscosity, ζ_d, is set equal to zero and the shear viscosity of μ_d =1 kg/ms is used. This value is based on data presented by Clift and Grace (1985). The solid pressure is expressed in terms of a particle-to-particle interaction coefficient referred to as the modulus of elasticity. It can be expressed as:

$$\nabla p_d = -G(a_c)\nabla a_c \tag{7}$$

There are various correlations for $G(\alpha_c)$ and the meaning and relevance of this modulus has been the subject of considerable discussion in the field (Massoudi et al., 1992). In this work the correlation of Ettehadieh et al. (1984) is applied.

$$G(a_d) = -10^{-10.46a_c + 6.577} \tag{8}$$

Kinetic theory of granular flow

The kinetic theory of granular flow model is based on the analogy between particles and the molecules of dense gases (Chapman and Cowling; 1970). An important difference is that the molecules in the dense gas are considered as elastic whereas the particles are inelastic causing kinetic energy dissipating into heat. The first models based on kinetic theory were not valid for dilute flows, as they did not account for the influence of the interstitial gas. This was first accounted for in the early 90's. The present model is based on the work of Ding and Gidaspow (1990) and Gidaspow (1994). The constitutive equations are summarized in Table 3.

Gas phase stress:

$$\bar{\boldsymbol{\tau}}_c = 2a_c m_c \bar{\mathbf{S}}_c \tag{9}$$

Solid phase stress:

$$\bar{\boldsymbol{\tau}}_d = \left(-p_d + a_d z_d\right)\bar{\mathbf{I}} + 2a_d m_d \bar{\mathbf{S}}_d \tag{10}$$

Deformation rate:

$$\bar{\mathbf{S}}_k = \frac{1}{2}\left(\nabla \mathbf{v}_k + (\nabla \mathbf{v}_k)^{\mathrm{T}}\right) - \frac{1}{3}(\nabla \cdot \mathbf{v}_k)\bar{\mathbf{I}} \tag{11}$$

Solid phase pressure:

$$p_d = a_d r_d \rho_s \left[1 + 2(1-e)a_d g_0\right] \tag{12}$$

Solid phase bulk viscosity:

$$z_d = \frac{4}{3} a_d r_d d_s g_0 (1+e)\sqrt{\frac{\Theta}{p}} \tag{13}$$

Solid phase shear viscosity:

$$m_d = \frac{2m_d^{\text{dilute}}}{a_d g_0 (1+e)}\left[1 + \frac{4}{5} a_d g_0 (1+e)\right]^2 + \frac{4}{5} a_d r_d d_s g_0 (1+e)\sqrt{\frac{\Theta}{p}} \tag{14}$$

Radial distribution function

$$g_0 = \left[1 - \left(\frac{a_d}{a_{d,\max}}\right)^{\frac{1}{3}}\right]^{-1} \tag{15}$$

Conductivity of the granular temperature:

$$\kappa_d = \frac{15}{2}\frac{m_d^{\text{dilute}}}{(1+e)g_0}\left[1 + \frac{5}{6} a_d g_0 (1+e)\right]^2 + 2a_d^2 r_d d_s g_0 (1+e)\sqrt{\frac{\Theta}{p}} \tag{16}$$

Collisional energy dissipation:

$$\gamma = 3(1-e^2)a_d^2 r_d \rho_s g_0 \Theta\left[\frac{4}{d_d}\sqrt{\frac{\Theta}{p}} - \nabla \cdot \mathbf{v}_d\right] \tag{17}$$

Table 3 Constitutive equations based on kinetic theory of granular flow.

Initial and boundary conditions

Initial conditions (t=0): Initially the bed is at rest and there is no gas flow in the reactor. The particle void fraction is slightly below maximum packing. When not assuming axi-symmetry, heterogeneity was introduced into the bed by creating a void area at the bottom of the bed towards the right boundary. This was done by setting the gas void fraction to unity. The effect of this void area has minor effects on the statistical behaviour of the fluid flow. The turbulent energy and dissipation rates as well as the granular temperature are low but non-zero.

Boundary conditions (t>0): The normal velocity component for both phases is set to zero at both boundaries. The wall boundary condition for the gas is based on the wall function approach consistent with the single-phase k-ε model. Assuming that the gas velocity profile near the wall is similar to that of single-phase flow, the skin friction coefficient can be obtained from the logarithmic part of the "law of the wall". The solids were allowed to slip along the wall, following the boundary conditions used by Ding and Gidaspow (1990):

$$v_{d,z}\big|_w = -\frac{d_p}{a_d^{1/3}}\frac{\partial v_{d,z}}{\partial r}\Big|_w \tag{18}$$

Uniform plug flow is assumed at the inlet. A prescribed pressure is specified at the outlet. The particles are not allowed to leave the reactor. For scalar variables, except for the pressure, Dirichlet boundary conditions are used at the inlet, whereas Neumann conditions are used at the other boundaries.

Chemical process

The chemical process implemented is the conversion of natural gas into synthesis gas. The kinetics is based on methane steam reforming with $Ni/MgAl_2O_3$ as the catalyst, where the most important reactions are:

$$CH_4 + H_2O = CO + 3H_2 \quad (19)$$

$$CO + H_2O = CO_2 + H_2 \quad (20)$$

$$CH_4 + 2H_2O = CO_2 + 4H_2 \quad (21)$$

The kinetics and correlations needed are taken from Froment and Bischoff (1990), De Groote and Froment (1995) and Xu and Froment (1989a,b). The operating conditions and boundary conditions used in the simulations as well as the data for the gas phase are given by Jakobsen et al. (2002). The inlet temperature and the temperature in the reactor are assumed constant and set to 1100 K.

NUMERICAL SOLUTION ALGORITHM

The algorithm applied in this work is based on the algorithm applied by Jakobsen et al. (2005). The governing two-fluid equations are discretized by a finite-volume algorithm. A staggered grid arrangement is used. A fractional-step scheme similar to those used by Tomiyama and Shimada (2001) and Lathouwers (1999) is developed on the basis of the single-phase algorithm reported by Jakobsen et al. (2002), Lindborg et al. (2004) and Jakobsen et al. (2005). The fractional steps defining the algorithm are sketched in the following discussion.

1. **Velocity prediction**
   Temporary velocity estimates are found by solving the momentum balances using implicit discretizations of the velocity variables:

$$\int_V \left(\frac{a_k^n r_k^n \mathbf{v}_k^* - a_k^n r_k^n \mathbf{v}_k^n}{\mathrm{D}t} \right) dv = - \int_V \nabla \cdot \left(a_k^n r_k^n \mathbf{v}_k^n \mathbf{v}_k^* \right) dv - \int_V a_k^n \nabla p^n \, dv + \int_V \nabla \cdot \bar{\boldsymbol{\tau}}_k^* \, dv + \int_V a_k^n r_k^n \mathbf{g}_k \, dv + \int_V \mathbf{M}_k^* \, dv \quad (22)$$

   The equations are solved by using a Partial Elimination Algorithm (PEA) in a coupled manner, though separately for each velocity direction.

2. **Void fraction prediction**
   Temporary void fractions are found by solving the dispersed phase continuity equation:

$$\int_V \left(\frac{a_d^* r_d^n - a_d^n r_d^n}{\mathrm{D}t} \right) dv = - \int_V \nabla \cdot \left(a_d^* r_d^n \mathbf{v}_d^* \right) dv \quad (23)$$

3. **Granular temperature prediction**
   In intermediate granular temperature is computed by use of temporary void fractions and velocity fields:

$$\int_V \frac{3}{2} \left[\frac{a_d^* r_d^n \theta^* - a_d^n r_d^n \theta^n}{\mathrm{D}t} \right] dv = - \int_V \frac{3}{2} \nabla \cdot \left(a_d^* r_d^n \mathbf{v}_d^{**} \theta^* \right) dv + \int_V \bar{\boldsymbol{\tau}}_d^{**} : \nabla \mathbf{v}_d^{**} dv + \int_V \nabla \cdot \left(k_{\theta_d} \nabla \theta^* \right) dv - \int_V 3 b^{**} \theta^* dv - \int_V g \, dv \quad (24)$$

   Since the source terms are all functions of the granular temperature, negative temperatures can be avoided by using positive source terms only on the right hand side of the discretized equation, while negative source terms are added to the center-coefficient. The particle pressure is then calculated based on the intermediate values of the void fractions and the granular temperature.

$$p_d^* = a_d^* r_d^n \theta^* \left[1 + 2(1+e) a_d^* g_0^* \right] \quad (25)$$

4. **Particle pressure- and velocity correction**
   The velocity of the dispersed phase is corrected due to change in particle pressure:

$$\int_V \left(\frac{a_d^* r_d^n \mathbf{v}_d^{**} - a_d^* r_d^n \mathbf{v}_d^*}{\mathrm{D}t} \right) dv = - \int_V \nabla dp_d \, dv + \int_V d\mathbf{M}_d \, dv \quad (26)$$

   where $dp_d = p_d^* - p_d^n$ and $d\mathbf{M}_d = \mathbf{M}_d^{**} - \mathbf{M}_d^*$. The velocity of the continuous phase is corrected due to velocity change of the dispersed phase velocity through the phase interaction term:

$$\int_V \left(\frac{a_c^* r_c^n \mathbf{v}_c^{**} - a_c^* r_c^n \mathbf{v}_c^*}{\mathrm{D}t} \right) dv = + \int_V d\mathbf{M}_c \, dv \quad (27)$$

   Solved with respect to the corrected velocity of the continuous phase gives:

$$\mathbf{v}_c^{**} = \frac{\left(a_c^n r_c^n \mathbf{v}_c^* - \mathrm{D}t \left(\mathbf{M}_c^* - b^{**} \mathbf{v}_d^{**} \right) \right)}{D} \quad (28)$$

where $D = a_c^* r_c^n + \Delta t b^n$. Inserting equation (28) into equation (26) solved with respect to the corrected velocity of the dispersed phase gives:

$$\mathbf{v}_d^{**} = \frac{\begin{pmatrix} a_d^n r_d^n \mathbf{v}_d^* \\ -\Delta t \tilde{N} dp_d + \Delta t \mathbf{M}_c^* \\ + \frac{\Delta t b^{**}}{D}\left(a_c^n r_c^n \mathbf{v}_c^* - \Delta t \mathbf{M}_c^*\right) \end{pmatrix}}{a_d^* r_d^n + \Delta t b^{**}\left(1 - \frac{\Delta t b^{**}}{D}\right)} \quad (29)$$

Point 3 and 4 are performed in an iteration procedure until the change in void fraction is less than a certain criterion.

5. **Gas pressure- and velocity correction**

A pressure update is then performed to update the pressure- and velocity-fields.

$$\int_V \left(\frac{a_k^* r_k^n \mathbf{v}_k^{n+1} - a_k^* r_k^n \mathbf{v}_k^{**}}{\Delta t}\right) dv = - \int_V a_k^* \tilde{N} dp\, dv \quad (30)$$

where $dp = p^{n+1} - p^n$. The equation for this update is found by introducing a time-independent volume fraction (and density) step.

Summation of the normalized continuity equations over both phases gives:

$$\sum_k \left(\frac{1}{r_k^0} \tilde{N} \cdot \left(a_k^* r_k^n \mathbf{v}_k^{n+1}\right)\right) = 0 \quad (31)$$

The transient term in the continuity equations cancels out as the sum of the volume fractions equals 1. Introducing the velocity correction $d\mathbf{v}_k = \mathbf{v}_k^{n+1} - \mathbf{v}_k^{**}$ into equation (31) results in:

$$\sum_k \left(\frac{1}{r_k^0} \tilde{N} \cdot \left(a_k^* r_k^n d\mathbf{v}_k\right)\right) = \sum_k \left(\frac{1}{r_k^0} \tilde{N} \cdot \left(a_k^* r_k^n \mathbf{v}_k^{**}\right)\right) \quad (32)$$

The velocity correction can be written in terms of a pressure correction. The pressure-velocity dependence can be obtained by subtracting a prediction step of the momentum equations from the semi-implicit discretization:

$$T_k d\mathbf{v}_k = - a_k^* \tilde{N} dp \pm b\left(d\mathbf{v}_d - d\mathbf{v}_c\right) \quad (33)$$

where $T_k = \frac{a_k^* r_k^n}{\Delta t}$. Rearranging with respect to the velocity correction gives for the continuous phase:

$$d\mathbf{v}_c = \frac{b d\mathbf{v}_d - a_c^* \tilde{N} dp}{T_c + b} \quad (34)$$

And for the dispersed phase:

$$d\mathbf{v}_d = \frac{b d\mathbf{v}_c - a_d^* \tilde{N} dp}{T_d + b} \quad (35)$$

Substituting the velocity correction in equation (35) with equation (34) gives the pressure-velocity dependence for the dispersed phase:

$$d\mathbf{v}_d = - \frac{a_d^* T_c + b}{T_c T_d + b\left(T_c + T_d\right)} \tilde{N} dp = - G_d \tilde{N} dp \quad (36)$$

For the continuous phase this gives:

$$d\mathbf{v}_c = - \frac{b G_d + a_c^*}{T_c + b} \tilde{N} dp = - G_c \tilde{N} dp \quad (37)$$

A Poisson equation is obtained after inserting the pressure velocity dependence into equation (32):

$$\sum_k \left(\frac{1}{r_k^0} \tilde{N} \cdot \left(a_k^* r_k^n G_k \tilde{N} dp\right)\right) = \sum_k \left(\frac{1}{r_k^0} \tilde{N} \cdot \left(a_k^* r_k^n \mathbf{v}_k^{**}\right)\right) \quad (38)$$

6. **Void fraction update**

The void fractions are updated by solving the continuity equation for the dispersed phase:

$$\int_V \left(\frac{a_d^{n+1} r_d^n - a_d^n r_d^n}{\Delta t}\right) dv = - \int_V \tilde{N} \cdot \left(a_d^{n+1} r_d^n \mathbf{v}_d^{n+1}\right) dv \quad (39)$$

7. **Granular temperature update**

The granular temperature is updated based on the new void fraction and velocity-fields:

$$\frac{3}{2}\left[\frac{a_d^{n+1} r_d^n \Theta^{n+1} - a_d^n r_d^n \Theta^n}{\Delta t}\right] = - \frac{3}{2} \tilde{N} \cdot \left(a_d^{n+1} r_d^n \mathbf{v}_d^{n+1} \Theta^{n+1}\right) + \bar{\boldsymbol{\tau}}_d^{n+1} : \tilde{N} \mathbf{v}_d^{n+1} + \tilde{N} \cdot \left(G_d \tilde{N} \Theta^{n+1}\right) - 3b\Theta^{n+1} - g \quad (40)$$

At the end a particle pressure-update is performed:

$$p_d^{n+1} = a_d^{n+1} r_d^n \Theta^{n+1} + 2(1 - e) a_d^{n+1} g_0^{n+1} \quad (41)$$

8. **Component mass fraction update**

Integrate the transport equations for the components in the gas phase. This is split into two steps. A convection-diffusion step:

$$\int_V \left(\frac{a_c^{n+1} r_c^n w_i^* - a_c^n r_c^n w_i^n}{\Delta t} \right) dv = - \int_V \nabla \cdot \left(a_c^{n+1} r_c^n \mathbf{v}_c^{n+1} w_i^* \right) dv + \int_V \nabla \cdot \left(a_c^{n+1} r_c^n D_{ea} \nabla w_i^* \right) dv \quad (42)$$

The final step is the reaction step:

$$\int_V \left(\frac{a_c^{n+1} r_c^n w_i^{n+1} - a_c^n r_c^n w_i^*}{\Delta t} \right) dv = \int_V R_i \, dv \quad (43)$$

9. **Density update**

When including compressibility in the gas phase, a density update is needed due to any eventual changes in temperature and fluid mixture composition. The density is then updated by using a suitable equation of state (EOS). In the case of an ideal gas:

$$\int_V r_c^* \, dv = \int_V \left(\frac{p^{n+1} M_m}{RT} \right) dv \quad (44)$$

The density at time step *n+1* is obtained from the gas phase continuity equation:

$$\int_V \left(\frac{a_c^{n+1} r_c^{n+1} - a_c^{n+1} r_c^*}{\Delta t} \right) dv = - \int_V \nabla \cdot \left(a_c^{n+1} r_c^{n+1} \mathbf{v}_c^{n+1} \right) dv \quad (45)$$

The fractional-step concept applied consists of successive applications of the predefined operators determining parts of the transport equation. The convective and diffusive terms are further split into their components in the various coordinate directions. The time-truncation error in the splitting scheme is of first order. The convective terms are solved using a second-order TVD scheme in space and a first-order explicit Euler scheme in time. The TVD scheme applied was constructed by combining the central difference scheme and the classical upwind scheme by adopting the "smoothness monitor" of van Leer (1974) and the monotonic centered limiter (van Leer; 1977).

All the linear equation systems are solved with preconditioned Krylov methods. A bi-conjugate gradient-solver (BCG) is applied for the granular temperature and the turbulent dissipation energy while a conjugate gradient-solver (CG) is used for the other variables. The solvers are preconditioned with a Jacobi preconditioner which is computationally very cheap and effective. In addition, compared to the more robust ILU preconditioner, it does not introduce any numerical perturbations.

Overview of the algorithm

- Velocity prediction. Solution of the momentum equations (22).
- Void fraction prediction using equation (23).
- Prediction of granular temperature using equation (24).
- Correction of particle pressure and velocities due to particle pressure correction (equations (25), (28) and (29).
- Correction of gas pressure and velocities using equation (38).
- Updating void fractions (equation (39)).
- Updating granular temperature (equation (40) and particle pressure (equation (41)).
- Calculating species composition (equation (4)).
- Updating the gas phase density.

SAMPLE RESULTS AND DISCUSSION

Simulations described in this work were performed for 25 s with a time step size of Δt=0.2 ms. Maximum Courant number is in the range 0.02 to 0.03. The results reported are averaged over the last 20 seconds to avoid influence of the start-up phase.

To validate the models, the simulation results have been compared with experimental results of Lin et al. (1985), who measured particle velocity in a cylindrical bed using a radioactive particle tracking method. The bed, 13.8 cm in diameter, contained glass Ballotini beads with diameters in the range of 0.42-0.60 mm, and a static bed height of 11.3 cm. In this work a particle diameter of 0.50 mm is assumed with a density of 2.5 g/cm^3. To compare the results with the work of Ding and Gidaspow (1990) and Pain et al. (2002) a uniform grid size of Δr=0.69 cm and Δz=1.13 cm was used. In addition, first order upwind discretization of convective terms is applied. Inlet superficial velocity of air was set as 64.1 cm/s, and a restitution coefficient value of 0.995 was used. The simulations are run in serial on an SGI Origin3800 with R14000 processors of 600MHz. A typical run on this grid size takes approximately 3800 CPU seconds when using the CPV model while the KTGF model is more computationally expensive with 5100 CPU seconds.

Results by using the KTGF model are shown in Figure 1. On average, the particles ascend at the center and descend near the wall. A vortex appeares in the upper portion between the center and the wall, as seen in the experimental results. However, the opposite directed vortex of lower velocities in the lower portion between the center and the wall seen in the experiments does not appear in the simulation results. Neither Ding and Gidaspow (1990) nor Pain et al. (2002) obtained these vortexes in their work (Figure 2).

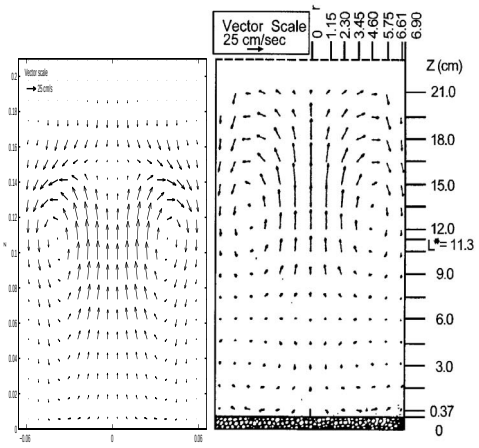

Figure 1 Computed (left) and experimental (right) solids velocities in cylindrical bed.

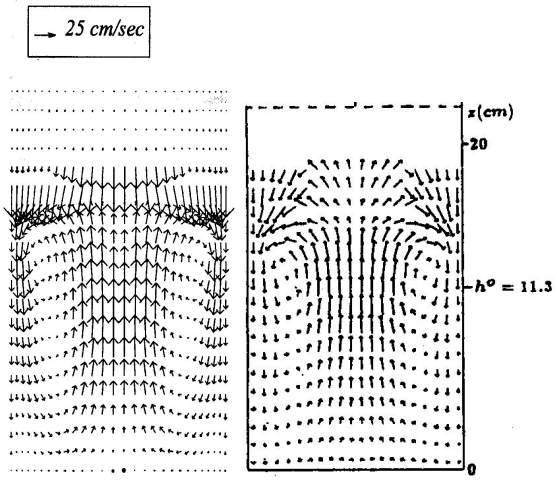

Figure 2 Solids velocities in cylindrical bed obtained by Pain et al. (2001 (left) and) Ding and Gidaspow (1990) (right).

On the other hand, the two oppositely directed vortexes are predicted by the CPV model, as shown in Figure 3. However, this model does not predict the correct particle motion at the center, as the particles tend to compact and descend quite fast in this region. The same motion is seen when applying two-dimensional Cartesian coordinates as shown in Figure 4. According to Sun and Gidaspow (1999) and Pain et al. (2001) some unrealistic high concentration of particles in the central region of the reactor can occur when applying axi-symmetrical boundary conditions, since the particles are prohibited from crossing the central axis. To overcome this problem, the symmetrical boundary conditions have to be removed and the whole domain has to be simulated where the symmetry is broken. It is common to insert some gas pockets asymmetrically into the bed initially or slightly tilt the gravity vector for a short period of time during start-up to break the symmetry. Special attention should be paid to the calculation of the coefficients and source terms of the equation systems as well as the solvers applied for solving them to avoid that the symmetry is broken by numerical perturbations originating from accuracy restrictions in the machine. The axi-symmetric boundary condition does however not always lead to unphysical flows. Ding and Gidaspow (1990) show that both cases are possible depending on flow rate, bed height and geometry.

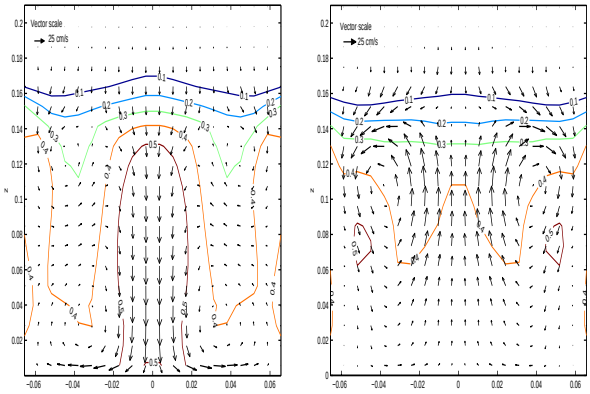

Figure 3 Computed solids void fractions and velocities in cylindrical bed obtained by using the CPV model (left) and the KTGF model (right).

The bed heights predicted by the two models are practically equal, but somewhat lower than observed in the experiments.

The solids motion obtained when simulating a rectangular axi-symmetric column using Cartesian coordinates does not qualitatively differ much from the motion obtained in the cylindrical column, although the highest velocities in the center are approximately 30% less when using the Cartesian coordinates. The ascending motion of the particles at the center predicted by the CPV model is not as dominant in the rectangular bed. The solids void fraction profiles predicted by this model do not change as much when changing coordinate system as they do when applying the KTGF model.

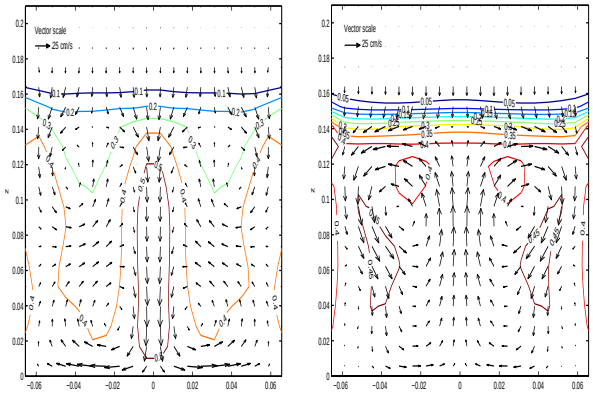

Figure 4 Computed solids void fractions and velocities in two-dimensional axi-symmetric bed obtained by using the CPV model (left) and the KTGF model (right).

Letting the particles cross the central axis, by removing the axi-symmetrical boundary conditions and introducing an asymmetric perturbation in the solids void fraction, results in profiles shown in Figure 5. Compared to the axi-symmetric simulations, there are minor changes in solids motion predicted by the KTGF model. However, it is

slightly asymmetric and the magnitude of the center-velocities is reduced by approximately 40%. There are also minor changes in void fraction profiles.

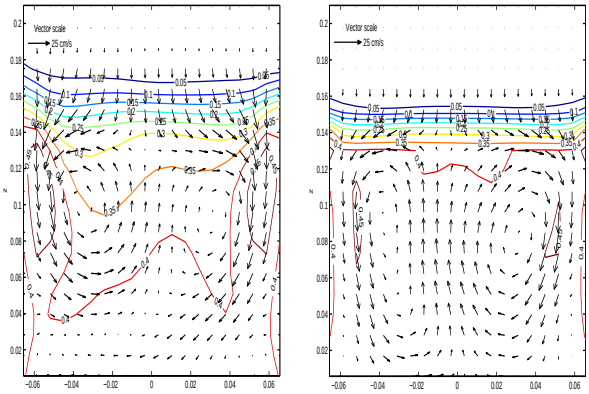

Figure 5 Computed solids void fractions and velocities in two-dimensional bed obtained by using the CPV model (left) and the KTGF model (right).

The solids motion predicted by the CPV model with and without axi-symmetrical boundary conditions differ a lot in the way that it is more similar to the results obtained with the KTGF model when the particles are allowed to cross the centerline. There is no region of high particle concentration at the center. The particles ascend at the center and descend near the wall creating two vortexes in the upper portion of the bed. In addition, there are no longer opposite directed vortexes in the upper and lower parts as in the axi-symmetric simulations. The predicted particle concentration in the upper half of the bed is somewhat lower than the concentration predicted by the KTGF model causing a more expanded bed.

Increased order on convective terms

Applying the TVD scheme with the monotonic centered limiter when solving the convection terms in the cylindrical bed, results in profiles shown in Figure 6. The major differences from the results obtained when using 1. order differentiation is an increased bed height which is in better agreement with the experimental results of Lin et al. (1985). The solids motion remains the same although the magnitudes of the velocities are higher. The CPV model predicts a more compact region along the central axis halfway up in the bed.

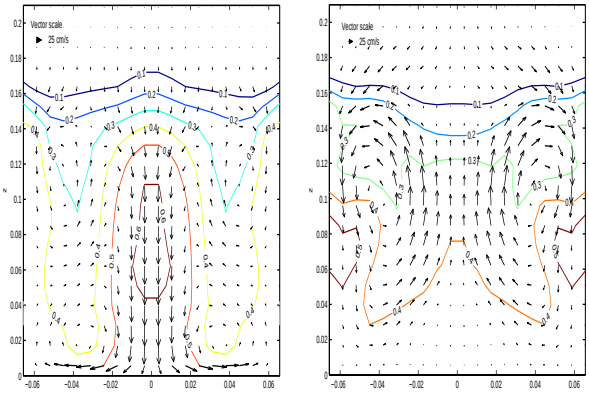

Figure 6 Computed solids void fractions and velocities in cylindrical bed obtained by using the CPV model (left) and the KTGF model (right). TVD scheme is applied when solving the convective terms.

Allowing the particles to cross the central axis gives the profiles shown in Figure 7. The solids velocity- and concentration profile obtained with the CPV model is fairly symmetric with up-flow in the center. The corresponding profiles obtained with the KTGF model appear to be more chaotic. An increase in discretization order of convective terms, and thereby a reduction in numerical diffusion seems to destabilize the solution. This effect is not seen with the CPV model as the shear viscosity is higher.

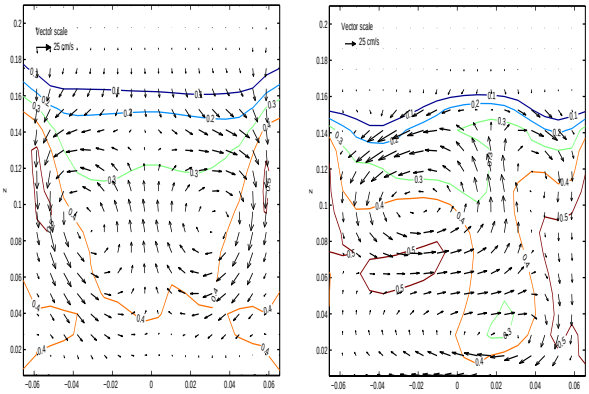

Figure 7 Computed solids void fractions and velocities in non-axi symmetric rectangular bed obtained by using the CPV model (left) and the KTGF model (right). TVD scheme is applied when solving the convective terms.

Synthesis gas production

The same physical data and fluid dynamic operating conditions are applied as for the cold flow simulations except for the outlet pressure which is 29 bars. The chemical model is turned on after 3 seconds to avoid influence of the start-up phase. Simulations of axi-symmetric columns resulted in heavy down flow of particles in the center. However, simulations of the non-axi symmetric rectangular column predicted ascending particles in the center as shown in Figure 8. Both models perform quite evenly both in predicting solids velocities and void fractions. The bed expansion is higher than in the cold flow simulations due to higher operating pressure and

different gas mixture. The components mass fractions were also predicted quite evenly by the two models. Thus, only the results from the KTGF model are shown in Figure 9. The mass fraction profile of the inert nitrogen gas, which is supposed to be flat, indicates how well the gas continuity equation is fulfilled. The discrepancies from the initial value of 0.0641 are small enough to avoid the error growing.

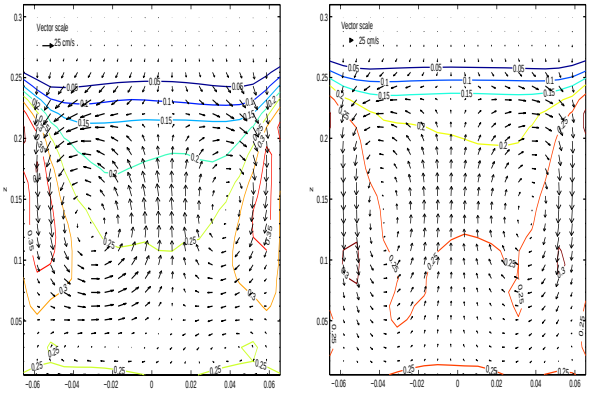

Figure 8 Computed solids void fractions and velocities in non-axi symmetric rectangular bed obtained by using the CPV model (left) and the KTGF model (right) when running the synthesis gas process.

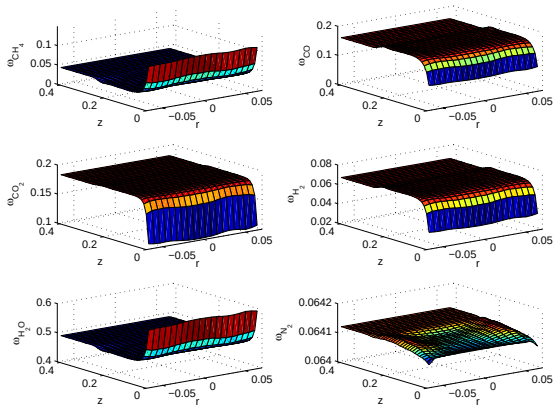

Figure 9 Mass fractions predicted when applying the KTGF model.

CONCLUSION

A numerical algorithm has been described for the solution of particle flow adopting an Eulerian modeling approach. Two closure models, the constant particle viscosity model (CPV) and a model based on kinetic theory of granular flow (KTGF), are compared in performance to describe the time-averaged velocity fields and bed expansion in both a circular and rectangular column. Axi-symmetric simulations of a cylindrical column using the KTGF model gives solids velocity profiles that are in fairly well agreement with experimental results obtained by Lin et al. (1985), while results obtained by using the CPV model give unrealistic high void fraction in the central region due to the axi-symmetric boundary conditions. Allowing the particles to cross the centerline causes the solids motions predicted by the two models to be more even. The predicted bed height is somewhat less than observed in the experiments. However, applying higher order discretizations of convective terms results in an increased bed expansion closer to the experimental results as long as the total diffusion is sufficiently high.

The inclusion of a chemical reacting system seems to perform satisfactorily. However, validation of the chemical process still remains.

ACKNOWLEDGEMENTS

This work has received support from the Research Council of Norway (Program of Supercomputing) through a grant of computer time.

REFERENCES

CHAPMAN, S. and COWLING, T.G., (1970), "The mathematical theory of non-uniform gases", Cambridge Mathematical Library, Cambridge, 3rd ed.

CLIFT, R. and GRACE, J.R., (1985), In: J.F. Davidson, R. Clift, D. Harrison (Eds.), "Fluidization", (Ch. 3, p. 77). London: Academic Press.

DE GROOTE, A.M. and FROMENT, G.F., (1995), "Reactor modeling and simulation in synthesis gas production", *Rev. Chem. Eng.*, **11**(2), 145-183.

DING, J. and GIDASPOW, D. (1990), "A bubbling fluidization model using kinetic theory of granular flow", *AlChE J.*, **42**(4), 927-931.

ENWALD, H, PEIRANO, E. and ALMSTEDT, A.E., (1996), "Eulerian two-phase flow theory applied to fluidization", *Int. J. Multiphase Flow*, **22**, 21-66.

ERGUN, S, (1952), "Fluid flow through packed columns", *Chem. Eng. Prog.*, **48**, 89-94.

FROMENT, G.F. and BISCHOFF, K.B., (1990), "Chemical reactor analysis and design", New York, Wiley.

GIDASPOW, D., (1994), "Multiphase flow and fluidization", Academic Press Inc., Boston, 1st ed.

JAKOBSEN, H.A., LINDBORG, H. and HANDELAND, V., (2002), "A numerical study of the interactions between viscous flow, transport and kinetics in fixed bed reactors". *Comput. Chem. Eng.*, **26**, 333.

JAKOBSEN, H.A., LINDBORG, H. and DORAO, C.A., (2005), "Modeling of Bubble Column Reactors: Progress and Limitations", *Ind. Eng. Chem. Res.*, ASAP Article.

LATHOUWERS, D. (1999), "Modeling and simulation of turbulent bubbly flow". Ph.D. Thesis, The Technical University of Delft, Delft, The Netherlands.

LAUX, H., (1998), "Modeling of dilute and dense dispersed fluid-particle flow", Ph.D. Thesis, NTNU, Trondheim, Norway.

LINDBORG, H., EIDE, V., UNGER, S., HENRIKSEN, S.T.; JAKOBSEN, H.A., (2004), "Parallelization and performance optimization of a dynamic PDE ractor model for practical applications", *Comput. Chem. Eng.* **28**, 1585.

MASSOUDI, M., RAJAGOPAL, K.R., EKMANN, J.M. and MATHUR, M.P., (1992), "Remarks on the modelling of fluidized systems", *AlChE J.*, **38**(3), 471-472.

PAIN, C.C., MANSOORZADEH, S., GOMES, J.L.M. and DE OLIVIERA, C.R.E., (2001), "A study of bubbling and slugging fluidised beds using the two-fluid granular temperature model", *Int. J. Multiphase Flow*, **27**, 527-551.

PAIN, C.C., MANSOORZADEH, S., GOMES, J.L.M. and DE OLIVIERA, C.R.E., (2002), "A numerical investigation of bubbling gas-solid fluidized bed dynamics in 2-D geometries", *Powder Technology*, **128**, 56-77

SAMUELSBERG, A. and HJERTAGER, B.H., (1996), "An experimental and numerical study of flow patterns in a circulating fluidized bed reactor", *Int. J. Multiphase Flow,* **22**, 575-591.

SUN, B. and GIDASPOW, D., (1999), "Computation of circulating fluidized-bed riser flow for the fluidization VIII benchmark test", *Ind. Eng. Chem. Res.*, **38**, 787-792.

TOMIYAMA, A. and SHIMADA, N. (2001), "A Numerical Method for Bubbly Flow Simulation Based on a Multi-Fluid Model". *J. Pressure Vessel Technol*., **23**, 510.

VAN LEER, B., (1974), "Towards the Ultimate Conservation Difference Scheme 2. Monotonicity and Conservation Combined in a Second-Order Scheme". *J. Comput. Phys.*, **14**, 361.

VAN LEER, B., (1977), "Towards the Ultimate Conservation Difference Scheme 4. A New Approach to Numerical Convection"., *J. Comput. Phys.* **23**, 276.

VAN WACHEM, B.G.M., SCHOUTEN, J.C., KRISHNA, R. and VAN DEN BLEEK, C.M., (1998), "Eulerian simulations of bubbling bed behaviour in gas-solid fluidised beds", *Comput, Chem. Eng.* **22**, 299-306.

WEN, Y.C. and YU, Y.H., (1966), "Mechanics of fluidization". *Chem. Eng. Prog. Symp. Series*, **62**, 100-111.

XU, J. and FROMENT, G.F., (1989a), "Methane steam reforming, methanation and water-gas shift. I. Intrinsic kinetics", *AIChE J.*, **35**(1), 88-96.

XU, J. and FROMENT, G.F., (1989b), "Methane steam reforming, methanation and water-gas shift. II. Diffusional limitations and reactor simulations", *AIChE J.*, **35**(1), 97-103.